The MyD88 inhibitor, ST2825, induces cell cycle arrest and apoptosis by suppressing the activation of the NF-κB/AKT1/p21 pathway in pancreatic cancer

SINAN LU[1,2*], TIANYU HE[2,3*], YUAN ZHANG[1,2*], BO ZHOU[1,2], QIYI ZHANG[1,2] and SHENG YAN[1,2]

[1]Department of Hepatobiliary and Pancreatic Surgery, The Second Affiliated Hospital, Zhejiang University School of Medicine; [2]Key Laboratory of Precision Diagnosis and Treatment for Hepatobiliary and Pancreatic Tumor of Zhejiang Province; [3]Department of Surgical Intensive Care Unit, The Second Affiliated Hospital, Zhejiang University School of Medicine, Hangzhou, Zhejiang 310009, P.R. China

Received February 24, 2023; Accepted May 3, 2023

DOI: 10.3892/or.2023.8585

Abstract. NF-κB activation occurs in the majority patients with pancreatic ductal adenocarcinoma (PDAC); however, directly targeting NF-κB has proven unsuccessful, and recent studies have demonstrated a certain effect of the indirect inhibition of NF-κB. Myeloid differentiation factor 88 (MyD88) is a common intermediate messenger for NF-κB activation by inducers. In the present study, the level of MyD88 in PDAC was detected using a public database and a tissue chip. A specific inhibitor (ST2825) of MyD88 was used on PDAC cell lines. Flow cytometry was used to examine apoptosis and cell cycle progression. Transcriptome sequencing was used for ST2825-treated PANC-1 cells compared with untreated PANC-1 cells. The levels of related factors were measured using reverse transcription-quantitative PCR and western blot analysis. Chromatin immunoprecipitation, co-immunoprecipitation, transcription factor assay and an NF-κB phospho-antibody array were performed to identify the detailed underlying mechanisms. Animal experiments were performed to verify the effects of ST2825 on PDAC, which were found in the *in vitro* experiments. MyD88 was found to be overexpressed in PDAC. ST2825 induced the G2/M phase cell cycle arrest and apoptosis of PDAC cells. ST2825 inhibited MyD88 dimerization to inactivate the NF-κB pathway. ST2825 inhibited AKT1 expression and induced p21 overexpression to induce G2/M phase cell cycle arrest and apoptosis by inhibiting NF-κB transcriptional activity. NF-κB activation, AKT1 overexpression or p21 knockdown partially reversed the effects of ST2825 in PDAC. On the whole, the findings of the present study demonstrate that ST2825 induces G2/M cell cycle arrest and apoptosis via the MyD88/NF-κB/AKT1/p21 pathway in PDAC. MyD88 may thus serve as a potential therapeutic target in PDAC. ST2825 may serve as a novel agent for the targeted therapy of PDAC in the future.

Introduction

Previous research has demonstrated that 80-90% of pancreatic cancer cases are pancreatic ductal adenocarcinoma (PDAC). In the present study, pancreatic cancer refers to PDAC. Pancreatic cancer mainly occurs in the head of the pancreas, accounting for >70% of all cases. The most common clinical symptom of pancreatic cancer is abdominal pain, often accompanied by jaundice and new-onset diabetes mellitus (1). Currently, surgery is the only available strategy used to eradicate pancreatic cancer. However, as the pancreas is located at the back of the abdomen, the symptoms of early-stage pancreatic cancer are not obvious and the majority of patients have already developed near invasion and distant metastasis at the time of diagnosis; thus, only a limited number of patients have the opportunity to receive surgery (2). Although PDAC has a low incidence, it constitutes the seventh leading cause of cancer-related mortality worldwide and the fourth leading cause of cancer-related mortality in the USA (3,4). Despite continuous improvements in tumor diagnosis and treatment strategies in general over the past several decades, and the notable progress in the 5-year survival rate of patients with certain tumor types, such as leukemia, the 5-year survival rate

Correspondence to: Professor Sheng Yan, Department of Hepatobiliary and Pancreatic Surgery, The Second Affiliated Hospital, Zhejiang University School of Medicine, 88 Jiefang Road, Hangzhou, Zhejiang 310009, P.R. China
E-mail: shengyan@zju.edu.cn

*Contributed equally

Abbreviations: PDAC, pancreatic ductal adenocarcinoma; TLR, Toll-like receptor; PanIN, human pancreatic intraepithelial neoplasia; RT-qPCR, reverse transcription-quantitative PCR; IL, interleukin; MyD88, myeloid differentiation factor 88; ChIP, chromatin immunoprecipitation; Co-IP, co-immunoprecipitation; GEPIA, gene expression profiling interactive analysis; TCGA, The Cancer Genome Atlas; IC50, half-maximal inhibitory concentration; IHC, immunohistochemical

Key words: MyD88, ST2825, pancreatic ductal adenocarcinoma, NF-κB, AKT1, p21

of patients with pancreatic cancer remains low (8.5%) in the USA (4).

Due to the poor efficacy of surgery for PDAC and the limited efficacy of recent chemotherapeutic regimens, the development of novel targeted drugs is of utmost importance. PDAC involves a number of mutated genes, including KRAS, BRCA2, INK4A, LκB1 and CDKN2A (5). Among these, the KRAS gene mutation exists in the majority of cases of advanced pancreatic cancer (6), which is most commonly found in codon 12 (7). Previous studies have indicated that the KRAS gene mutation is one of the earliest genetic events in the progression of human pancreatic intraepithelial neoplasia (PanIN) (8,9). At first, due to the universality and importance of KRAS mutations in pancreatic cancer, a number of small molecule inhibitor studies targeting mutant RAS protein have been performed; however, to date, these have proven unsuccessful (10). Researchers have tried to identify the signal transduction pathways which play a vital role downstream of RAS, in order to inhibit the occurrence and development of PDAC by suppressing these pathways (11). NF-κB is constitutively activated in the majority (67-70%) patients with PDAC (12,13), which can promote cell proliferation, angiogenesis and invasion (14). Thus, NF-κB is considered a highly promising target for PDAC treatment. However, directly targeting NF-κB proteins by small-molecule inhibitors has proven unsuccessful for >30 years (15-17); however, efforts against potential NF-κB inducers [such as tumor necrosis factor (TNF)-α, interleukin (IL)-1α and Toll-like receptor (TLR) family members] have achieved some effects (18-20).

TLR and IL-1 family receptors are key molecules for human cells to recognize microorganisms or endogenous ligands and inflammatory mediators, which play a vital role in the activation of the NF-κB pathway (21). Ling *et al* (22) revealed that KrasG12D-activated AP-1 induced IL-1α, which activated NF-κB and its target genes, IL-1α and p62, to initiate IL-1α/p62 feedforward loops for inducing and sustaining NF-κB activity. Furthermore, IL-1α overexpression was shown to be associated with Kras mutation, NF-κB activity and the poor survival in of patients with PDAC. Zhang *et al* (23) demonstrated that the IL-1 receptor-associated kinase 4 (IRAK4), the master kinase that relays signaling downstream of TLRs, was activated in human PDAC samples and positively correlated with activated NF-κB, which was associated with a high post-operative relapse and a poor patient survival. Therefore, MyD88, as the common intermediate messenger for NF-κB activation by these inducers, may play a vital role in PDAC therapy.

Myeloid differentiation factor 88 (MyD88) MyD88 is a member of the TLR/IL-1R family and the death domain family; apart from TLR3, they all transmit signals through MyD88 (24). MyD88 is a soluble cytoplasmic protein with three functional domains. The N-terminus is a domain with 90 amino acid residues, mainly mediating interactions between proteins containing dead sequences. The C-terminus Toll and intermediate regions, which contain 130 amino acid residues, mainly transmit signals by recruiting junction proteins. Previous studies have demonstrated that an elevated MyD88 expression promotes tumor growth and metastasis via TLR/IL-1R signaling in hepatocellular carcinoma (HCC) and is related to the low survival rate of patients with PDAC (25,26). Zhu *et al* (27) revealed that blocking MyD88 signaling markedly attenuated the development of PDAC-associated cachexia. MyD88-dependent inflammation is crucial in the pathophysiology of pancreatic cancer progression and contributes to a high mortality rate (27). Thus, it was hypothesized that MyD88 inhibition, potentially via the specific MyD88 small molecule inhibitor, ST2825 (28), which has been shown to inhibit HCC cell proliferation and promote cell apoptosis (29), may serve as an effective target strategy for PDAC.

In order to identify factors and strategies with which to enhance the efficacy of PDAC chemotherapeutics, the present study aimed to determine the role of MyD88 in PDAC and whether MyD88 inhibition by ST2825 would suppress the progression of PDAC. Furthermore, the present study investigated whether NF-κB activation plays a vital role in the effects of ST2825, and also aimed to identify the underlying signaling pathways.

Materials and methods

Tissues, cell lines and reagents. A tissue chip of PDAC and paracancerous tissues (HPanAde170Sur01) was obtained from Shanghai Outdo Biotech Co., Ltd. The human PDAC cell lines, AsPC-1 (ATCC cat. no. CRL-1682, RRID:CVCL_0152), BxPC-3 (ATCC cat. no. CRL-1687, RRID:CVCL_0186), CFPAC-1 (ATCC cat. no. CRL-1918, RRID:CVCL_1119), PANC-1 (ATCC cat. no. CRL-1469, RRID:CVCL_0480) and hTERT-HPNE (ATCC cat. no. CRL-4023, RRID:CVCL_C466) were purchased from the American Type Culture Collection. All cells were maintained in RPMI-1640 medium containing 10% fetal bovine serum (Thermo Fisher Scientific, Inc.) and cultured at 37˚C in an atmosphere of 5% CO_2. The drugs, activators and inhibitors used included ST2825 (HY-50937) and IL-1α (HY-P7027) from MedChem Express.

Cell interference and transfection. The cells were cultured in six-ell plates with 3 μl short interfering RNA (siRNA) and 7 μl Lipofectamine 3000® (Thermo Fisher Scientific, Inc.) for 6 h. The siRNA, named p21(h)-si-1,2,3 (si-1, 5'-GCGATG GAACTTCGACTTTGT-3'; si-2, 5'-GCTCTACATCTTCTG CCTTAG-3'; si-3, 5'-GCAGACCAGCATGACAGATTT-3') was designed and synthesized by GenePharma Co., Ltd. The AKT1 recombinant plasmids were designed and synthesized by Ruibo Bio-Technology Co., Ltd. and were used following the manufacturer's protocol. The AKT1 recombinant lentivirus was designed and synthesized by Hanbio Biological Technology Co. The PANC-1 cells were counted the day prior to viral infection; 10,000 cells were inoculated in a well of a 12-well plate and cultured overnight at 37˚C. The virus was diluted with serum-free medium, and added in the 12-well plate for infection. The number of viruses was added according to the recommended infection MOI for PANC-1 cells (MOI=10). Following 6 h of infection using 3 μl Polyjet reagent (SignaGen Laboratories), the solution containing the virus was removed and RPMI-1640 medium containing 10% fetal bovine serum was added for cell culture. Following 48 h of culture at 37˚C the fluorescence intensity of the cells was observed under a fluorescence microscope (LEXT OLS4100, Olympus Corporation). At the same time, 3 μg/ml puromycin (HY-B1743A, MedChem Express) was added for cell screening,

which lasted for ~2 weeks. After cell screening, reverse transcription-quantitative PCR (RT-qPCR) and western blot analysis were performed to detect the stable expression of the target gene.

Nuclear and cytoplasmic extraction and western blot analysis. The nuclear and cytoplasmic extraction reagents were utilized according to the manufacturer instructions (NE-PER™, cat. no. 78833, Thermo Fisher Scientific, Inc.). Total proteins were then extracted from the cells by incubating in RIPA cell lysis buffer with 1% PMSF and phosphatase inhibitors (Wuhan Servicebio Technology Co., Ltd.) on ice for 30 min. Following centrifugation (1,000 x g, 4˚C, 5 min), the supernatant was collected. Nuclear and cytoplasm extracts were collected using Nuclear and Cytoplasmic Extraction Reagents (NE-PER™, Thermo Fisher Scientific, Inc.). The cells were pelleted and re-suspended in 400 ml cold Buffer A at 4˚C. The cells were set on ice for 10 min and then vortexed for 10 sec. Following centrifugation (1,000 x g, 4˚C, 5 min), the supernatant fraction was saved as crude cytoplasm extract. The pellet was re-suspended in 20 to 100 ml cold Buffer C basing on the starting number of cells and incubated on ice for 20 min for high-salt extraction. Nuclear and cytoplasm extracts were collected and cleared by centrifugation. Subsequently, 30 μg total/nuclear/cytoplasm protein were measured using a BCA protein assay kit (Thermo Fisher Scientific, Inc.). The proteins were then separated using 4-12% SurePAGE Bis-Tris gels [Gen Script (Nanjing) Co., Ltd.] at consistent 120 V for 60 min. The separated proteins were then transferred onto PVDF membranes at consistent 350 mA for 60 min. Following transfer, the membrane was blocked using 5% BSA solution for 2 h at 4˚C, followed by overnight incubation at 4˚C with the following primary antibodies. Antibodies against the following proteins were used: GAPDH, Lamin B1, p21, p53, MyD88, p100, p105 (all from Abcam); Bax, Bcl-2 (Proteintech, Rosemont, IL, USA); Cdk1, phosphorylate-Cdk1, Cyclin B1, Chk1, phosphorylated-Chk1, phosphorylated-AKT1, AKT1, phosphorylated-p65, p65, Caspase-3, cleaved Caspase-3, PARP, cleaved PARP (Cell Signaling Technology, Inc.); and p50, p52, IKKα and IKKβ (Santa Cruz Biotechnology, Inc.). Target proteins were detected by anti-mouse or anti-rabbit antibodies for 1 h at room temperature. Detection was carried out using the ECL kit (Wuhan Servicebio Technology Co., Ltd.). Visualization was performed using the ChemiDoc MP system (Bio-Rad Laboratories, Inc.). The grayscale detection of protein bands was completed using Image Lab 6.1 software (Bio-Rad Laboratories, Inc.). GAPDH was used to normalize the protein expression. The detailed research resource identifiers (RRIDs), catalogue numbers and dilutions of the antibodies are presented in Table SI.

RT-qPCR. TRIzol® reagent (Thermo Fisher Scientific, Inc.) was used for the extraction of total RNA from the cells. NanoDrop ND-1000 UV/visible photometer (Thermo Fisher Scientific, Inc.) was used to assess RNA purity. Reactions were performed using the ChamQ universal SYBR master mix (Vazyme Biotech) in the Bio-Rad CFX96 RealTime System. Pre-incubation at 95˚C for 120 sec, amplification at 40 cycles of 95˚C for 30 sec, 60˚C for 30 sec and 72˚C for 30 sec and then a final extension at 72˚C for 5 min. mRNA expression was calculated using the $2^{-\Delta\Delta Cq}$ method (30). Shanghai Biological Engineering Technology Co. designed and synthesized all primers used (5'-3') (Table SII). All data were normalized relative to GAPDH.

ST2825 and IL-1α treatment. As, to the best of our knowledge, ST2825 has never been used in PDAC cell lines prior to the present study, the concentration of ST2825 used herein was based on the overall consideration of the manufacturer's certificate (MedChem Express) and previous studies. *In vitro*, the working concentration of ST2825 used in previous studies (28,29,31) ranged from 2 to 30 μmol/l, and was mainly 5 and 10 μmol/l. In order to determine the accurate IC50 value, a gradient of 0 to 80 μmol/l (0, 5, 10, 20, 40 and 80 μmol/l) was set. The PDAC cells was treated with 5 or 10 μmol/l of ST2825 for 24 h prior to use in further experiments, apart from the colony formation assay. *In vivo*, previous study (28) demonstrated that animals were orally administered ST2825 at doses ranging from 50 to 200 mg/kg, or intraperitoneally at a dose of 25 mg/kg daily in 7 days. According to the information provided, in the present study, the animals were intraperitoneally injected with ST2825 on days 7, 10, 13, 16, 19 and 22 at a dose of 20 mg/kg. The concentration of IL-1 α (10 ng/ml) used in PANC-1 cells were based on a previous study (19).

Flow cytometry for apoptosis and cell cycle analysis. Apoptosis and the cell cycle were detected using a Digital BD LSR II flow cytometer (BD Biosciences). The apoptosis of the cells was detected using an Annexin V-FITC/PI apoptosis detection kit (BD Biosciences). The cells were collected and suspended with binding buffer (BD Biosciences), then mixed with 5 μl fluorescein isothiocyanate-labeled Annexin V and 5 μl propidium iodide to detect apoptosis. The cells in Q2 and Q4 were considered as apoptotic cells. In the examination of cell cycle progression, cells were collected and preserved in 75% alcohol for 24 h, and then mixed with cell cycle liquid (BD Biosciences) to examine cell cycle distribution.

3-(4,5-Dimethyl-2-thiazolyl)-2,5-diphenyl-2-H-tetrazolium bromide (MTT) assay for measuring the IC50 values. The cells were seeded in 96-well plates ($4x10^3$ cells per well). The attached cells were treated with ST2825 (0, 5, 10, 20, 40 and 80 μmol/l) 24 h later. Following 48 h of incubation at 37˚C, an MTT kit (C11019-2; Ruibo Bio-Technology Co., Ltd.) was used to measure active cells, and the absorbance was then detected at 570 nm using an iMark™ Microplate Absorbance Reader (Bio-Rad Laboratories, Inc.).

Colony formation assay. The cells were cultured at 10,00 cells per 10 cm dish. The cells were then treated with 1 μmol/l ST2825 for 2 weeks. The colonies were fixed with formalin (MilliporeSigma) within 30 min and stained with Wright-Giemsa dye (Nanjing Jiancheng Yuehao Technology Co., Ltd.) within 1 h at 37˚C and counted using an inverted phase contrast microscope (IX79, Olympus Corporation).

Transcriptome sequencing and analysis. The negative control and 5 μmol/l ST2825-treated (48 h) PANC-1 cells were collected and prepared for sequencing. The expression of mRNA between the two groups was compared and analyzed,

including genome mapping, differential expressed gene screening and Kyoto Encyclopedia of Genes and Genomes (KEGG) pathway enrichment analysis. The detailed procedures were performed as previously described (32).

Histological and immunohistochemical (IHC) analyses. The PANC-1 cell slides in six-well plates were fixed in 4% formalin (MilliporeSigma) for 15 min and washed with PBS twice. The cells were permeabilized with 0.5% Triton X-100 (Beijing Solarbio Science & Technology Co., Ltd.) for 15 min and blocked with 5% BSA solution (Beyotime Institute of Biotechnology) for 1 h. The cells were then incubated with primary antibodies against phosphorylated-p65 (1:200, ab86299, Abcam,) overnight at 4˚C after blocking non-specific binding. The cells were then washed with PBS three times and stained with the anti-rabbit secondary antibody (1:10,000, ab205718, Abcam) and counterstained with DAPI (1:1,000, 5 μg/ml, ab104139 Abcam) to visualize the nuclei. The slides were observed using a fluorescence microscope (LEXT OLS4100, Olympus Corporation) and imaged. The sections of tumors from the nude mice used in the present study (as described below) were stained with antibodies against MyD88 (ab133739, Abcam, 1:500, rabbit), phosphorylated-p65 (ab86299, Abcam, 1:100, rabbit), phosphorylated-AKT1 (4060, Cell Signaling Technology, Inc., 1:100, rabbit) or p21 (ab54562, Abcam, 1:500, mouse). Briefly, the PDAC tissues were excised 1 day after the collection of tumors. The tissue sections were formalin-fixed, paraffin-embedded and subjected to immune-staining using the streptavidin-peroxidase technique. The sections were then subjected to heat with 0.01 mol/l citrated buffer (Beyotime Institute of Biotechnology) and incubated at 4˚C overnight with the primary antibodies. The slides were washed by Tris-buffered saline buffer (Beyotime Institute of Biotechnology) and incubated for 30 min with the anti-rabbit secondary antibody (1:10,000, ab205718, Abcam,) or anti-mouse secondary antibody (1:10,000, ab205719, Abcam,) before being counterstained with Meyer's hematoxylin for 5 min at 37˚C (Beyotime Institute of Biotechnology). The slides were observed using a confocal microscope (FV3000, Olympus Corporation). The PDAC tissue chip was stained with antibodies against myd88 from Outdo Biotech Company, Shanghai, China (HPan-Ade170Sur-01). All procedures performed in studies involving human participants were in accordance with the ethical standards of the Shanghai Outdo Biotech Company Ethics Committee and with the 1964 Declaration of Helsinki and its later amendments or comparable ethical standards mentioned in the product description. The tissues mentioned above were all subjected to IHC staining using a previously described method (19). Tissue sections were scanned using Pannoramic MIDI (3D HISTECH). H-SCORE=$\sum$ (PI xI)=(percentage of cells of weak intensity x1) + (percentage of cells of moderate intensity x2) + percentage of cells of strong intensity x3). The staining results were evaluated by two experienced pathologists in a double-blinded manner.

ELISA and phosphorylation chip assessment. PANC-1 cell nuclear fractions were isolated and the binding activity of NF-κB with dsDNA was examined using an NF-κB p65 Transcription Factor Assay kit (ab133112, Abcam) following the manufacturer's protocol. The PANC-1 cells were treated with 0 and 5 μmol/l ST2825 for 48 h. The cell lysates were collected, added to an NF-κB Phospho-Antibody Array (PCS248, Full Moon BioSystems), and detected by Wayen Biotechnologies Inc. according to the manufacturer's protocol. The analysis method was carried out as previously described (33).

Chromatin immunoprecipitation (ChIP) and co immunoprecipitation (Co-IP). The PANC-1 cells were treated with 0 and 5 μmol/l with ST2825 for 48 h. The MAGnify™ Chromatin Immunoprecipitation System (cat. no. 492024, Thermo Fisher Scientific, Inc.) was used to detect the p65-DNA interaction (p65-*AKT1*, p65-*CDKN1A* and p65-*CCND-1*), as previously described (34). Co-IP was performed using the Pierce Crosslink Immunoprecipitation kit (cat. no. 26147, Thermo Fisher Scientific, Inc.) as previously described (33). Flag-MyD88 and Myc-MyD88 plasmids were designed and provided by Wuhan Genecreate Biological Engineering Co. For transfection, the cells were inoculated in a 10-cm cell culture dish the day prior to transfection, with a cell density of 70-80% at the time of transfection and a culture medium of DMEM + 10% FBS. A total of 60 μl transfection reagent PEI diluted to 800 μl medium, 20 μg (Flag-MyD88 and Myc-MyD88, per 10 μg) diluted to 800 μl medium was then added, and mixed and incubated at room temperature for 20 min, and replenished to 3 ml. The culture medium was removed from the dish, and 3 ml transfection complex was prepared as in the previous step, and incubated at 37˚C for 5-6 h. The culture medium was removed and replaced with 2 ml complete culture medium and incubated at 37˚C for 48 h. Rat anti-human Flag (cat. no. SAB4200071, MilliporeSigma, 2.5 μg/ml) and mouse anti-human Myc (cat. no. M4439, MilliporeSigma, 2.5 μg/ml) antibodies were used to incubate with pre-treated proteins at 4˚CC overnight for immunoprecipitation.

Animal experiments. All mice were housed in accordance with the guidelines of the Zhejiang Medical Experimental Animal Care Commission. A total of 10 male (BALB/C, 5 weeks old) and 24 female nude mice (BALB/C, 5 weeks old) were provided by the Key Laboratory of Precision Diagnosis and Treatment for Hepatobiliary and Pancreatic Tumor of Zhejiang Province. The mice were housed in groups (5 or 6 mice per cage) in a specific-pathogen-free room with filtered air and controlled temperature (24±2˚C), relative humidity (45-65%) and light/dark cycle (12/12 h), and water and food were adequately provided. In the animal experiment with 10 male mice, $1x10^6$ PANC-1 cells were injected into each mouse subcutaneously in the axillary region on day 0, and the mice were randomly divided into two groups (negative control and ST2825 group; 5 mice per group). ST2825 was intraperitoneally injected on days 7, 10, 13, 16, 19 and 22 at a dose of 20 mg/kg. In the animal experiment with 24 female mice, the animals were randomly divided into four groups (negative control, ST2825, ST2825 after IL-1α and ST2825 + AKT1 groups; 6 mice per group). A total of $1x10^6$ PANC-1 cells were injected into each mouse subcutaneously in the axillary region on day 0. The PANC-1 cells used in the ST2825 after IL-1α group were

Table I. Analysis of the clinical characteristics of the 64 patients from the PDAC tissue chip.

Characteristic	Low-MyD88 group (n=32)	High-MyD88 group (n=32)	P-value
Sex			0.6107
Male	20	18	
Female	12	14	
Age, years			0.3513
>50	27	24	
≤50	5	8	
Tumor size, cm			0.0417[a]
>4	9	15	
≤4	23	17	
TMN stage			0.1329
I-IIA	20	14	
IIB-IV	12	18	
Tumor differentiation			0.6056
I-II	21	19	
III	11	13	

The data are presented as the mean ± SD; the Chi-squared test was used for data analysis, [a]P<0.05.

pre-treated with 10 ng/ml IL-1α for 1 week prior to injection; the PANC-1 cells used in the ST2825 + AKT1 group were transfected with AKT1 recombinant plasmids 24 h prior to injection. ST2825 was intraperitoneally injected on days 7, 10, 13, 16, 19 and 22 at a dose of 20 mg/kg. All mice were observed for body weight and tumor volume within 4 weeks and were then sacrificed by cervical dislocation; the condition of the animals and their tumors were examined every 3 days, and the tumors were weighed and collected for IHC analyses. All animal experiments were approved by the Zhejiang Medical Experimental Animal Care Commission. The humane endpoints were set as follows: i) A tumor burden >10% of body weight, in an adult mouse; a tumor should not exceed 20 mm in any dimension; ii) the tumor cannot not reach a position that severely affects the normal functioning of the animal, or the growth of the tumor causes animal pain; iii) the weight loss of animals exceeded 20% of their normal body weight (taking into account the proportion of tumors); iv) ulcers or infections at tumor growth points; v) tumor metastasis to other tissues and organs; vi) persistent spontaneous damage caused by tumor growth; vii) tumor growth interfered with dietary activities. In the present study, 1 mouse reached the fourth humane endpoint, and the mouse was sacrificed immediately following the observation of the ulcer and the data of the mice were excluded.

Gene expression profiling interactive analysis (GEPIA). GEPIA (http://gepia.cancer-pku.cn/) was used in the present study to examine the expression of MyD88 in various types of cancer. The correlation between the expression level of MyD88 with that of RELA, RELB, REL, NFκB1, NFκB2, AKT1 and CDNK1A was examined. In addition, the overall and disease-free survival plots were analyzed depending on the expression level of MyD88 in PDAC.

Statistical analysis. SPSS Statistics 19 software (SPSS, Inc.) was used for all statistical analyses. Data are presented as the mean ± SD. The t-test was used to analyze significant differences when only two groups were being compared at the same time, and the Bonferroni test was used for the multiple comparisons. For the Kaplan-Meier analysis, the hazard ratio was calculated based on the Cox PH Model with a 95% confidence interval, the log-rank test was used to identify significant differences between the two groups. Pearson's correlation analysis was used for the correlation analysis. The Chi-squared test was used for categorical ordinal data in Table I. All statistical tests were two-sided and P<0.05 was considered to indicate a statistically significant difference.

Results

MyD88 is highly expressed in PDAC and indicates a worse clinical outcome; MyD88 inhibitor ST2825 suppresses tumor growth in vitro and in vivo. Based on GEPIA [and The Cancer Genome Atlas (TCGA) database], the MyD88 gene expression profile across all tumor samples and paired normal tissues revealed a significantly higher MyD88 expression in PDAC (named as PAAD in Fig. S1) than in normal tissue (Figs. 1A and S1). To investigate the association between MyD88 and the clinical outcomes of patients with PDAC, the association between MyD88 expression and the survival rate in GEPIA was analyzed. The overall survival rate was longer in the low MyD88 group, but did not significantly differ from that in the high MyD88 group (Fig. 1B, P=0.14), whereas the disease-free survival rate in the low MyD88 group was significantly longer (Fig. 1C, P=0.0074). MyD88 protein expression was further detected using IHC in a PDAC tissue chip containing 64 pairs of tumor and paracancerous tissues with available clinical information for patients, including survival time. MyD88 expression was significantly

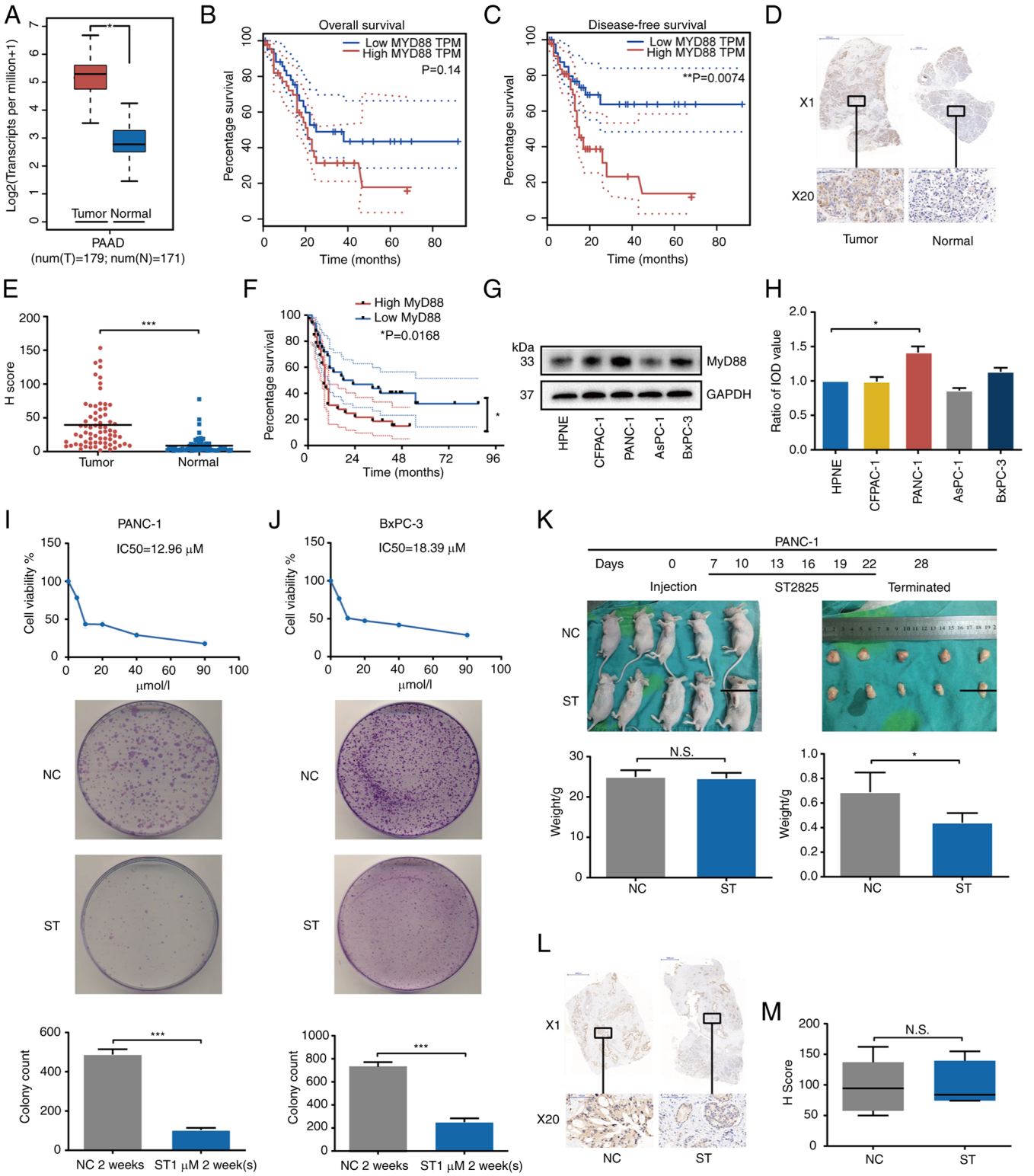

Figure 1. MyD88 is highly expressed in PDAC and indicates a worse clinical outcome. The MyD88 inhibitor, ST2825, suppressed tumor growth *in vitro* and *in vivo*. (A) Gene expression of MyD88 in PDAC (n=179) and paracancerous tissues (n=171) from TCGA database. (B and C) Overall survival time and disease-free survival time of the patients in the high MyD88 group (n=45) compared with those in the low MyD88 group (n=45) from TCGA database. (B and C) Overall survive time and disease-free survive time of the high MyD88 group (N=45) compared with the low MyD88 group (n=45) from the TCGA database. (D and E) Immunohistochemical staining and H-score of MyD88 in PDAC and paracancerous tissues from the tissue chip (n=64). (F) Overall survival time of the high MyD88 group (n=32) compared with the low MyD88 group (n=32) from the tissue chip. (G and H) Western blot analysis of the expression of MyD88 in HPNE, CFPAC-1, PANC-1, AsPC-1 and BxPC-3 cell lines. (I and J) MTT assay was used to determine the IC50 values and colony formation assay was used to determine the growth of PANC-1 and BxPC-3 cell lines treated with ST2825. (K) Image of each nude mouse and its hypodermic tumor, body/tumor weight changes in the mice treated with the negative control and ST2825. (L and M) Immunohistochemical staining (x1 and x20 magnification) and H-score of MyD88 in tissues of the negative control and ST2825 groups. All experiments were performed in triplicate (apart from the animal experiments) and the data are presented as the mean ± SD. The t-test was used for statistical analysis, *P<0.05, **P<0.01 and ***P<0.001; N.S., not significant. PDAC, pancreatic ductal adenocarcinoma; MyD88, myeloid differentiation factor 88; IC50, half maximal inhibitory concentration; PAAD, pancreatic adenocarcinoma; NC, negative control; ST, ST2825.

higher in the tumor tissues compared with the normal tissues (Fig. 1D and E). Depending on the MyD88 IHC score in the tumor tissues, the 64 patients were divided into two groups. Kaplan-Meier analysis demonstrated that patients with a lower MyD88 expression (32 patients) exhibited a significantly longer overall survival time than those with a higher MyD88 expression (32 patients) (Fig. 1F, P=0.0168). Further analysis of the patient clinical information revealed that the tumor size differed significantly between the two groups, being larger in the group with a high MyD88 expression (Table I).

In a panel of four human PDAC cell lines and HPNE (a type of immortalized human pancreatic epithelial cell line), the PANC-1 and BxPC-3 cells expressed higher levels of MyD88 protein than the HPNE cells, as determined using western blot analysis, exhibiting a significant difference compared to the PANC-1 cells (Fig. 1G and H). Therefore, the PANC-1 and BxPC-3 cells were selected as the main experimental cell line for use in further experiments. Following treatment with 5, 10, 20, 40 and 80 μmol/l ST2825, and MTT assay, the IC50 value of ST2825 in the PANC-1 cells was found to be 12.96 μmol/l (Fig. 1I, top panel), and that in the BxPC-3 cells was found to be 18.39 μmol/l (Fig. 1J, top panel). To examine the effects of ST2825 on cell proliferation, a colony formation assay were performed following treatment of the PANC-1 and BxPC-3 cells with 1 μmol/l ST2825; the results revealed that ST2825 significantly inhibited the growth of the PDAC cells (Fig. 1I and J, bottom panels). In addition, to examine whether ST2825 inhibits PDAC tumor growth *in vivo*, 10 BALB/C nude mice were injected hypodermically with $1x10^6$ PANC-1 cells and randomly divided into two groups (n=5 per group). The tumors were lobulated, hard in texture and appeared grayish white or light yellowish white in color, with unclear boundaries with their surrounding tissues. Tumors from the mice in the ST2825 group treated with ST2825 were significantly smaller than those in the negative control group, whereas no significant difference was observed in mouse body weight between the two groups (Fig. 1K). Furthermore, IHC analysis of the tumor xenografts revealed that MyD88 expression did not differ significantly between the two groups (Fig. 1L and M).

The MyD88 inhibitor, ST2825, induces the cell cycle arrest and apoptosis of PDAC cells. To examine the effects of ST2825 on PDAC cells, alterations in the cell cycle and apoptosis of PANC-1 and BxPC-3 cells following treatment with 0, 5 and 10 μmol/l ST2825 were examined using flow cytometry. The ratio of cells at the G2/M phases in the three groups of PANC-1 cells (negative control, 5 and 10 μmol/l ST2825) was 12.99±1.45, 54.54±0.99 and 86.93±3.37%, respectively (Fig. 2A and B), and in the BxPC-3 cells this was 7.87±1.29, 12.10±3.51 and 54.63±6.07%, respectively (Fig. 2C and D), which revealed that ST2825 treatment significantly arrested the PANC-1 and BxPC-3 cells at the G2/M phase with the increasing ST2825 concentration. The ratio of apoptotic cells in the three groups of PANC-1 cells (negative control, 5 and 10 μmol/l ST2825) was 4.97±1.20, 12.70±2.17 and 37.60±5.10%, respectively (Fig. 2E and F), and that in the BxPC-3 cells was 4.33±0.80, 7.37±0.51 and 11.47±0.76%, respectively (Fig. 2G and H), which revealed that ST2825 treatment induced significant PDAC cell death by apoptosis in a concentration-dependent manner.

To confirm the aforementioned results, the levels of cell cycle arrest- and apoptosis-related proteins were examined using western blot analysis. The levels of Cdk1 and Cyclin B1 and other related protein levels (the Cdk1-Cyclin B1 complex), acting as the key promoter of the G2-to-M phase progression, were evaluated. Cdk1 expression was significantly decreased, while Cyclin B1 expression was increased with the increasing ST2825 concentration. The expression of phosphorylated Chk1 was increased while that of Chk1 was decreased, which phosphorylated cdk1 to reduce the level of the Cdk1-Cyclin B1 complex (Figs. 2I and J, and S2). Furthermore, p21 expression was significantly increased concomitant with a decrease in p53 expression, which may underlie the significant G2/M phase cell cycle arrest upon Cdk1 decline (Fig. 2I and J). Moreover, the levels of pro-apoptotic proteins (such as cleaved PARP, cleaved caspase-3 and Bax) increased with the increasing ST2825 concentration, as shown by western blot analysis, whereas the level of Bcl-2 (a type of apoptosis inhibitory protein) significantly decreased (Figs. 2K and L, and S2).

ST2825 inhibits MyD88 dimerization to inactivate the NF-κB pathway in PDAC cells. To investigate the detailed underlying mechanisms of the effects of ST2825 on MyD88, the PANC-1 and BxPC-3 cells were treated with 0, 5 and 10 μmol/l ST2825. The expression of MyD88 was not significantly altered, as shown by RT-qPCR and western blot analysis (Fig. 3A and B); both the mRNA and protein levels of MyD88 were not markedly altered following treatment with ST2825. As MyD88 expression in PDAC cells was unaltered by ST2825, to confirm whether ST2825 inhibits MyD88 by dedimerization, plasmids with Flag-MyD88 and Myc-MyD88 were constructed, which were then transfected into PANC-1 and BxPC-3 cells. As the expression of Flag and Myc was higher in the PANC-1 cells than in the BxPC-3 cells (as determined using western blot analysis), the PANC-1 cells were selected for use in further co-IP experiments (Fig. 3C). The Flag-complex was then collected by co-IP and the components were detected by western blot analysis. ST2825 treatment decreased the Myc-myd88 level in a concentration-dependent manner (Fig. 3D), indicating that ST2825 inhibited MyD88 dimerization to inactivate MyD88 in PDAC cells, which was consistent with the previously published mechanism in 293T cells (28).

To reveal the molecular pathway involved in the effects of ST2825 transcriptome sequencing of normal and ST2825-treated PANC-1 cells was performed. The results of cluster analysis revealed that ST2825 mRNA expression was altered in PANC-1 cells (Fig. 3E). KEGG enrichment analysis indicated that the NF-κB signaling pathway was distinctly inhibited in the ST2825-treated PDAC cells (Fig. 3F). In addition, the correlation between MyD88 expression and members of the NF-κB signaling pathway, including RELA (p65), RELB (RelB), REL (c-Rel), NFκB1 (p50), NFκB2 (p52), CHUK (IKKα) and IκBκB (IKKβ) was analyzed in GEPIA; the MyD88 mRNA level significantly positively correlated with all of these genes (Fig. S3). To confirm these results, RELA (key gene of the NF-κB signaling pathway) expression was examined using RT-qPCR and western blot analysis in the PANC-1 and BxPC-3 cells. The RELA mRNA level was significantly

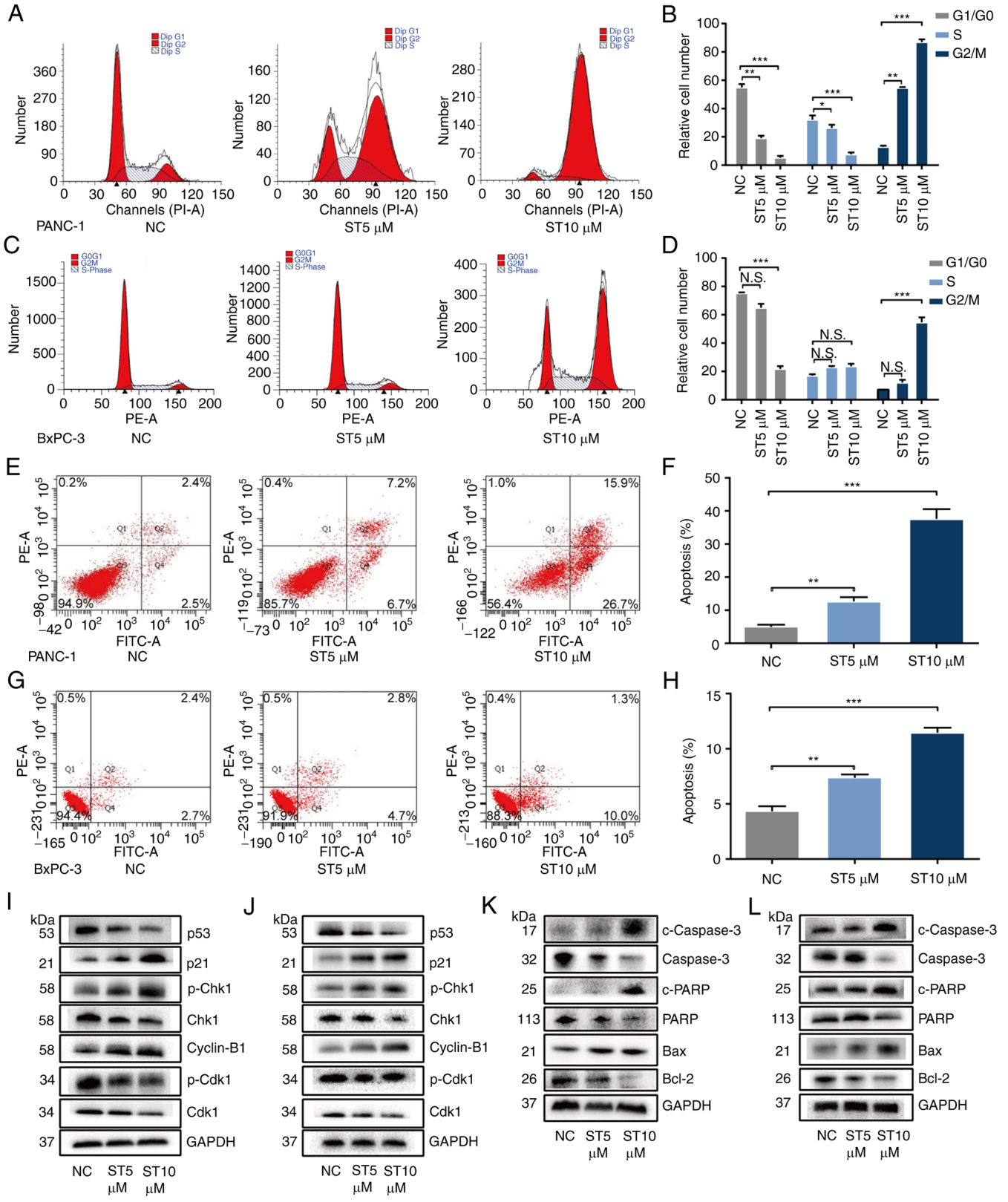

Figure 2. The MyD88 inhibitor, ST2825, induces the cell cycle arrest and apoptosis of PDAC cells. (A and B) Flow cytometric analysis of the cell cycle to determine the changes in the ratio of PANC-1 cells in the G0/G1, S and G2/M phases following treatment with ST2825. (C and D) Flow cytometric analysis of the cell cycle to determine the changes of the ratio of BxPC-3 cells in the G0/G1, S, and G2/M phases following treatment with ST2825. (E and F) Flow cytometric analysis in the Annexin V-FITC/PI apoptosis assay to determine the ratio of apoptotic PANC-1 cells following treatment with ST2825. (G and H) Flow cytometric analysis in the Annexin V-FITC/PI apoptosis assay to determine the ratio of apoptotic BxPC-3 cells following treatment with ST2825. (I and J) Western blot analysis of the three groups of PANC-1/BxPC-3 cells as in panels A and C to determine the changes of expression of cell cycle-related proteins. (K and L) Western blot analysis of the three groups of PANC-1/BxPC-3 cells as in panels E and G to determine the changes in the expression of apoptosis-related proteins. All experiments were performed in triplicate and the data are presented as the mean ± SD. The t-test with the Bonferroni test was used for statistical analysis, *P<0.05, **P<0.01 and ***P<0.001; N.S., not significant. PDAC, pancreatic ductal adenocarcinoma; MyD88, myeloid differentiation factor 88; NC, negative control; ST, ST2825.

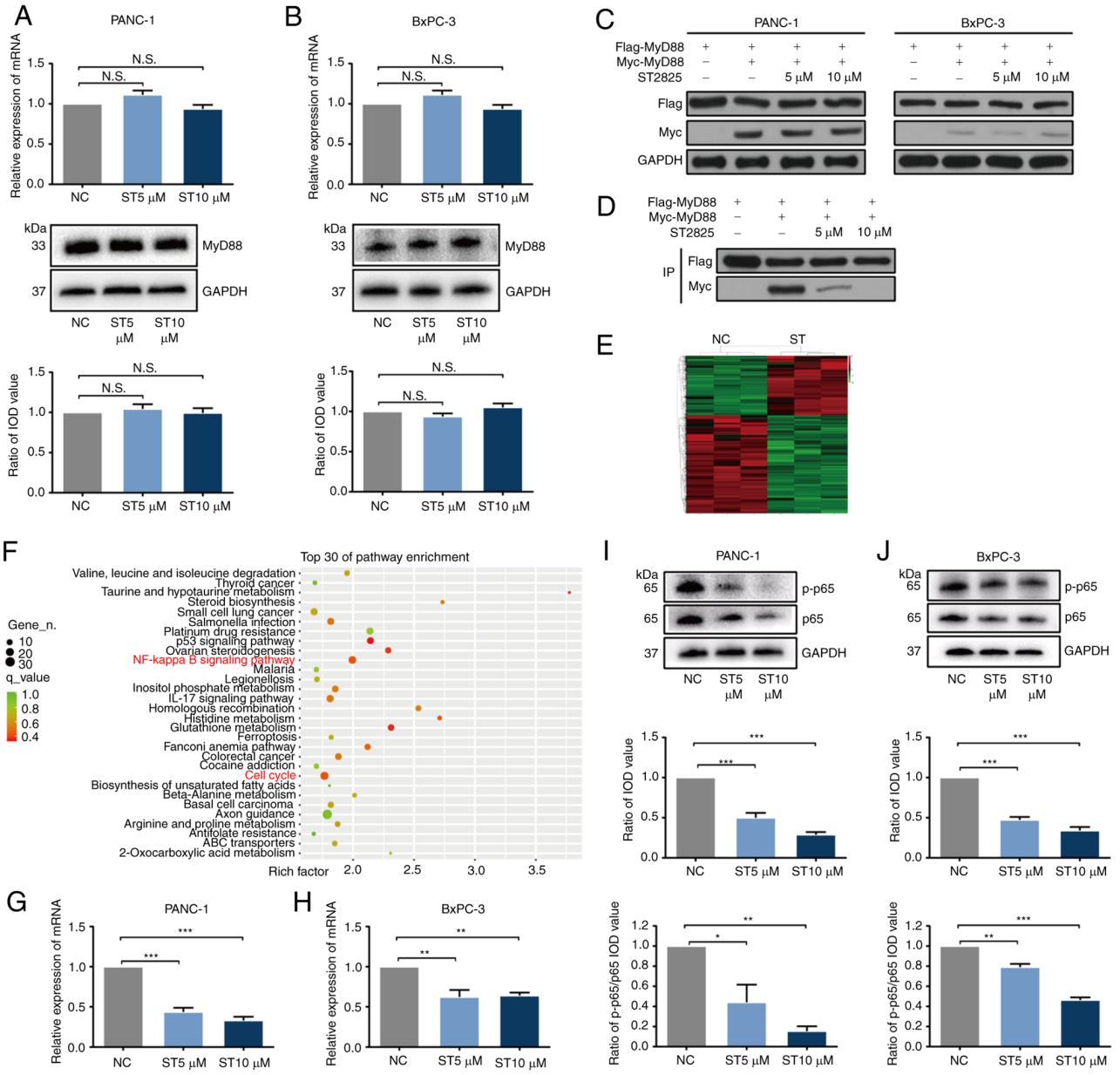

Figure 3. ST2825 inhibits MyD88 dimerization to inactivate the NF-κB pathways in pancreatic ductal adenocarcinoma cells. (A and B) RT-qPCR and western blot analysis were used to determine the relative expression of MyD88 in PANC-1 and BxPC-3 cells treated with ST2825. (C) Western blot analysis was used to determine the expression of myc and Flag following transfection with plasmids of Myc-MyD88 and Flag-MyD88 in PANC-1 and BxPC-3 cells treated with ST2825. (D) Western blot analysis was used to determine the expression of Myc-MyD88 from the co-IP of Flag-complex following transfection with plasmids of Myc-MyD88 and Flag-MyD88 in PANC-1 cells treated with ST2825. (E and F) Hierarchical clustering and Kyoto Encyclopedia of Genes and Genomes enrichment analysis based on the expression profiles of significantly differentially expressed proteins between negative control and ST2825 groups of the PANC-1 cells. (G and H) RT-qPCR analysis was used to determine the relative expression of RELA(p65) in PANC-1 and BxPC-3 cells treated with ST2825. (I and J) Western blot analysis was used to determine the expression of p65, phosphorylated-p65 and the ratio of phosphorylated-p65/p65 in PANC-1 and BxPC-3 cells treated with ST2825. All experiments were performed in triplicate and the data are presented as the mean ± SD. The t-test with the Bonferroni test was used for statistical analysis, *P<0.05, **P<0.01 and ***P<0.001; N.S., not significant. MyD88, myeloid differentiation factor 88; RT-qPCR, reverse transcription-quantitative PCR; NC, negative control; ST, ST2825.

decreased (Fig. 3G and H), and the p65 level was significantly decreased as was the ratio of phosphorylated-p65/p65 proteins with the increasing ST2825 concentration (Fig. 3I and J), indicating that ST2825 decreased p65 expression concomitantly with p65 dephosphorylation.

ST2825 inhibits AKT1 expression and induces p21 overexpression by inhibiting NF-κB transcriptional activity in PDAC cells. Based on the obtained data, it was suggested that inhibition of the NF-κB pathway constituted the main mechanism of action of ST2825. A series of experiments were then performed to investigate whether ST2825 inhibits NF-κB (as a classic transcription factor family) activity. To investigate whether ST2825 inhibits the entry of activated NF-κB proteins into the nucleus, the PANC-1 cells were treated with 0, 5 and 10 μmol/l ST2825.Western blot analysis revealed that ST2825 decreased the content of phosphorylated-p65 and other vital NF-κB proteins, including p52,

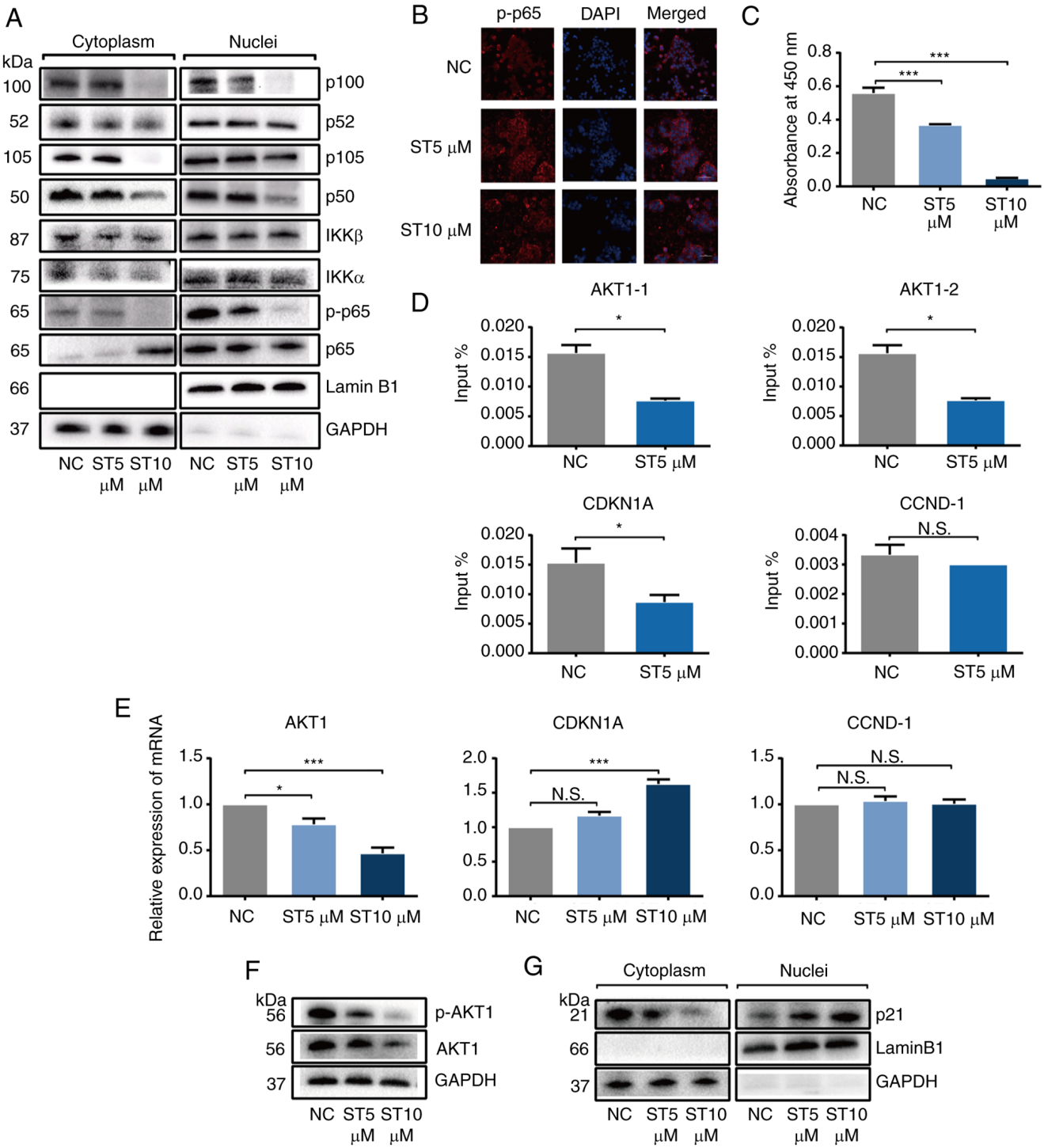

Figure 4. ST2825 inhibits AKT1 expression and induces p21 overexpression by inhibiting the transcriptional activity of NF-κB in pancreatic ductal adenocarcinoma cells. (A) Western blot analysis was used to determine the expression of NF-κB family proteins in the cytoplasm and nuclear extracts of PANC-1 cells treated with ST2825. (B) Immunostaining results of phosphorylated-p65 and DAPI in PANC-1 cells treated with ST2825 as imaged by confocal microscopy. (C) Value of the absorbance at 450 nM of nuclear p65/dsDNA ELISA in PANC-1 cells treated with ST2825. (D) RT-qPCR analysis was used to determine the expression of AKT1, CDKN1A(p21) and CYCLIN D1 from the ChIP of p65-complex in PANC-1 cells treated with ST2825. (E) RT-qPCR analysis was used to determine the expression of AKT1, CDKN1A(p21) and CYCLIN D1 in PANC-1 cells treated with ST2825. (F) Western blot analysis was used to determine the expression of AKT1 and phosphorylated-AKT1 in PANC-1 cells treated with ST2825. (G) Western blot analysis was used to determine the expression of p21 in the cytoplasm and nuclear extracts of PANC-1 cells treated with ST2825. All experiments were performed in triplicate and the data are presented as the mean ± SD. The t-test and Bonferroni test were used for statistical analysis, $^{*}P<0.05$ and $^{***}P<0.001$; N.S., not significant. p, phosphorylated; RT-qPCR, reverse transcription-quantitative PCR; NC, negative control; ST, ST2825.

p50, IKKα and IKKβ in the nuclear extracts in a concentration-dependent manner, indicating that ST2825 inhibited NF-κB activation through both canonical and non-canonical pathways (Fig. 4A). Confocal microscopy imaging of the immunostaining results confirmed that ST2825 inhibited the intranuclear protein content of phosphorylated-p65 in

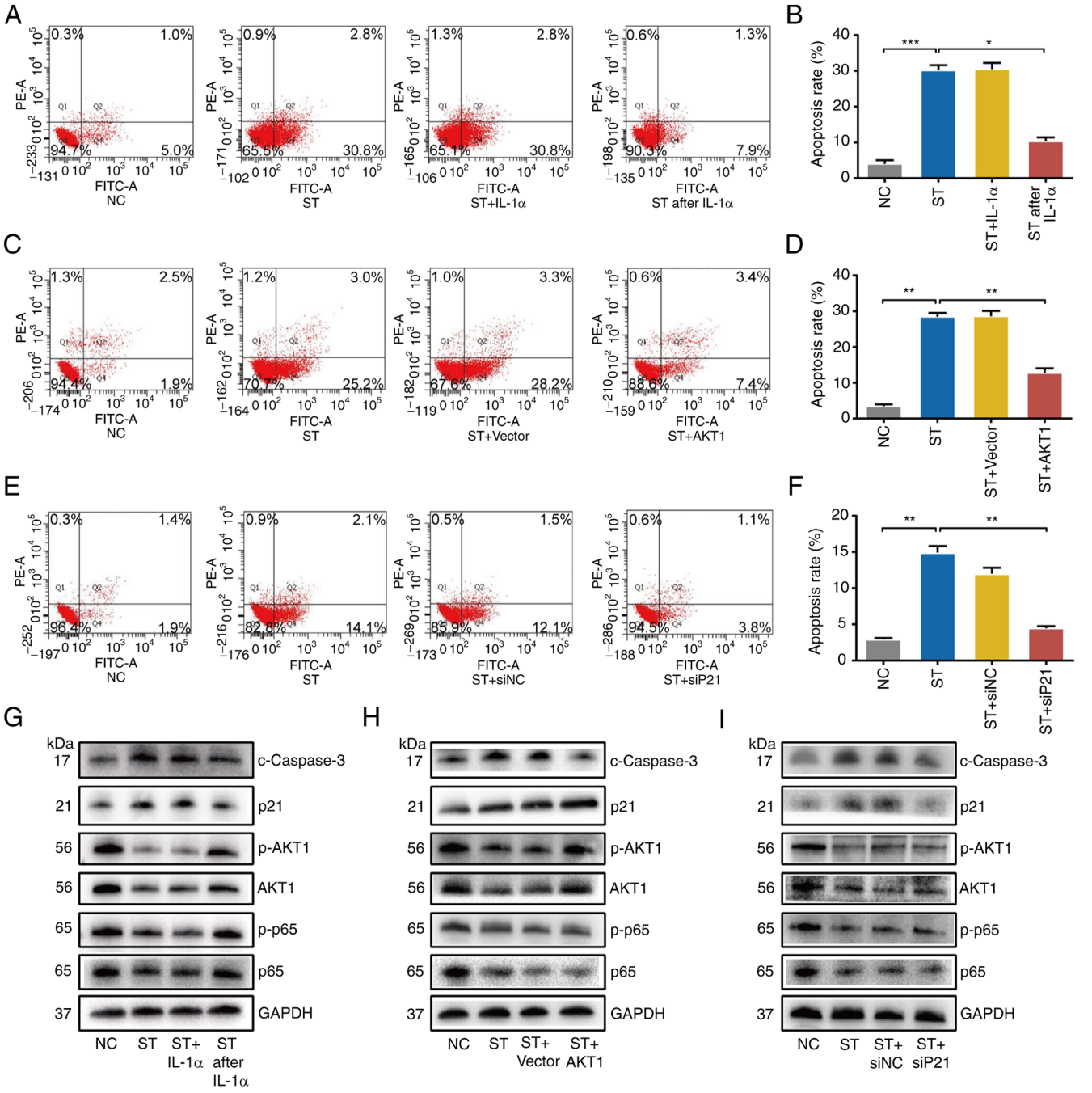

Figure 5. NF-κB activation, AKT1 overexpression or p21 knockdown partially reverses the effects of ST2825 on pancreatic ductal adenocarcinoma cells. (A and B) Flow cytometric analysis in the Annexin V-FITC/PI apoptosis assay to determine the ratio of apoptotic PANC-1 cells following ST2825 treatment combined with IL-1α. (C and D) Flow cytometric analysis in the Annexin V-FITC/PI apoptosis assay to determine the apoptotic ratio of PANC-1 cells following ST2825 treatment combined with control or AKT1 plasmids. (E and F) Flow cytometric analysis in the Annexin V-FITC/PI apoptosis assay to determine the ratio of apoptotic PANC-1 cells following ST2825 treatment combined with control or p21 siRNAs. (G-I) Western blot analysis was used to determine the changes in expression of related proteins in PANC-1 cells of the groups mentioned in panels A, C and E. All experiments were performed in triplicate and the data are presented as the mean ± SD. The t-test and Bonferroni test were used for statistical analysis, *P<0.05, **P<0.01 and ***P<0.001. NC, negative control; ST, ST2825.

a concentration-dependent manner (Fig. 4B). Moreover, to clarify the binding ability of NF-κB protein and its targeted DNA, the PANC-1 cells were treated with ST2825 and the extracted nuclear protein was examined using an NF-κB/p65 Transcription Factor Assay kit. The results demonstrated that ST2825 significantly decreased the binding ability of p65 and dsDNA in a concentration-dependent manner (Fig. 4C).

Subsequently, the authors wished to determine the vital target genes of NF-κB which underlie the effects of ST2825. Based on the results of transcriptome sequencing mentioned above (Table SIII) and a NF-κB phosphorylation chip analysis (Table SIV), AKT1 and CDKN1A (p21) were selected as key target gene candidates for NF-κB. The ChIP analysis revealed that treatment with 5 μmol/l ST2825 significantly inhibited p65 binding to AKT1 and CDKN1A, but did not alter the

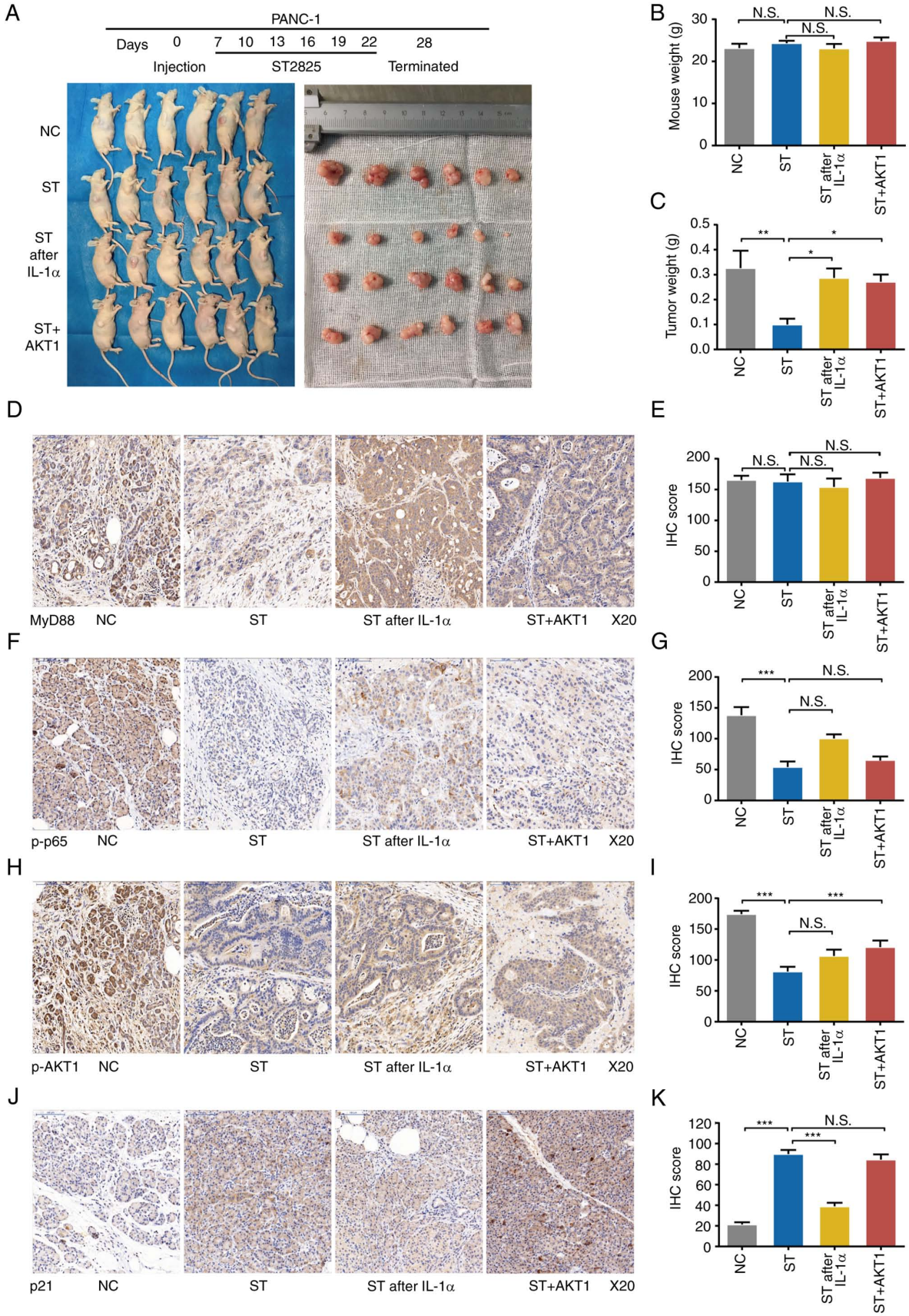

Figure 6. Activation of NF-κB or overexpression of AKT1 antagonizes the inhibitory effects of ST2825 on pancreatic ductal adenocarcinoma cells *in vivo*. (A) Image of each nude mouse and its hypodermic tumor in four groups (the mice treated with negative control, ST2825, ST after IL-1α and ST + AKT1). (B and C) Body weight and tumor weight changes of the groups in panel A. (D and E) IHC analysis of MyD88 expression in the tumors of the groups in panel A. (F and G) IHC analysis of phosphorylated-p65 expression in the tumors of the groups in panel A. (H and I) IHC analysis of phosphorylated-AKT1 expression in the tumors of the groups in panel A. (J and K) IHC analysis of p21 expression in the tumors of the groups in panel A. The data are presented as the mean ± SD. The t-test and Bonferroni test were used for statistical analysis, $^{*}P<0.05$, $^{**}P<0.01$ and $^{***}P<0.001$; N.S., not significant. IHC, immunohistochemical; NC, negative control; ST, ST2825.

binding ability of p65 to CCND-1 (as a known p65 binding gene), suggesting that ST2825 selectively affected downstream genes of NF-κB (Fig. 4D). Moreover in GEPIA, the MyD88 mRNA level significantly and positively correlated with AKT1 and CDKN1A (Fig. S3).

The present study then examined the expression of candidate downstream NF-κB targeting genes using RT-qPCR and western blot analysis following ST2825 treatment. The result of RT-qPCR revealed a significantly decreased AKT1 and an increased CDKN1A expression with the increasing ST2825 concentration; however, the level of CCND-1 was not altered (Fig. 4E). The protein levels of AKT1 and phosphorylated-AKT1 were decreased (Figs. 4F and S2) and that of p21 was increased as aforementioned (Fig. 2I and J) with the increasing ST2825 concentration. Furthermore, western blot analysis revealed that the p21 content increased in the nuclear extracts, whereas it decreased in the cytoplasmic extracts following treatment with ST2825 in a concentration-dependent manner (Fig. 4G). A previous study reported that phosphorylated-AKT1 inhibited p21 from entering the nucleus to induce cell cycle arrest (35). The results mentioned above indicated that ST2825 promoted p21 entry into the nucleus to induce G2/M phase cell cycle arrest followed by apoptosis by decreasing AKT1 expression concomitantly with p21 overexpression.

NF-κB activation, AKT1 overexpression or p21 knockdown partially reverse the effects of ST2825 on PDAC cells. To confirm the role of the NF-κB/AKT1/p21 pathway for in the observed phenomena, a series of rescue experiments were performed. The PANC-1 cells were treated with 10 μmol/l ST2825 with a combination of IL-1α as a NF-κB activator. The results of Annexin V-FITC/PI assay revealed that when the PDAC cells were concurrently treated with a combination of IL-1α (10 ng/ml) and ST2825, cell apoptosis was not lower than that following treatment with ST2825 alone. However, when IL-1α (10 ng/ml) was added 24 h prior to ST2825 treatment, it significantly reversed apoptosis induced by ST2825 (Fig. 5A and B). Western blot analysis confirmed that the latter treatment reversed the effects on p65, phosphorylated-p65, AKT1, phosphorylated-AKT1, p21 and cleaved Caspase-3 expression induced by ST2825 (Fig. 5G).

Furthermore, recombinant plasmid was used to overexpress AKT1 (Fig. S4). This was then transfected into PANC-1 cells with a combination of 10 μmol/l ST2825. The results of Annexin V-FITC/PI assay demonstrated that the increasing ratio of apoptotic cells induced by ST2825 was partially reversed by AKT1 overexpression (Fig. 5C and D). Western blot analysis revealed that AKT1 overexpression also reversed the effects on akt1, phosphorylated-akt1 and cleaved caspase-3, but not those on p65, phosphorylated-p65 and p21 induced by ST2825 (Fig. 5H).

Subsequently, siRNA-p21-1, 2 and 3 were used to knock down the expression of p21 in PANC-1 cells (Fig. S4). The mixture of siRNA-2 and 3 was selected for use in further experiments. The expression p21 was knocked down using siRNA with a combination of 5 μmol/l ST2825 treatment in PANC-1 cells. Flow cytometry revealed that the ST2825-induced G2/M phase arrest and subsequent apoptosis were partially reversed by p21 knockdown (Figs. 5E and F, and S4). Western blot analysis also revealed that p21 knockdown reversed the effects of ST2825 on p21 and cleaved Caspase-3, but not on p65, phosphorylated-p65, AKT1 and phosphorylated-AKT1 (Fig. 5G). Taken together, these data indicated that the NF-κB/AKT1/p21 pathway played a vital role in the effects of ST2825 on PDAC, and AKT1 and p21 were the key downstream factors of NF-κB.

NF-κB activation or AKT1 overexpression antagonizes the inhibitory effects of ST2825 on PDAC cells in vivo. To confirm the mechanisms of the ST2825-mediated inhibition of PDAC cells *in vivo*, 24 mice were hypodermically injected with $1x10^6$ PANC-1 cells and randomly assigned to four groups (negative control, ST2825, ST2825 after IL-1α, and ST2825 + AKT1; 6 mice per group) in an ectopic xenograft nude mouse model. Recombinant lentivirus was used to establish a stable akt1-overexpressing PANC-1 cell line (Fig. S4). Consistent with the results obtained *in vitro*, the tumor weight was evidently smaller following ST2825 treatment alone than following the combined treatments (Fig. 6A). The weight of the nude mouse did not differ significantly among all four groups (Fig. 6B), whereas tumor weights in the ST2825 group were significantly smaller than those in the other three groups (Fig. 6C).

Furthermore, IHC analysis of the tumor xenografts revealed that MyD88 expression did not differ significantly between the four groups (Fig. 6D and E). The decrease in the phosphorylated-p65 level in the ST2825 group compared with the negative control groups was partially reversed in the ST2825 after IL-1α group, but not in the ST2825 + AKT1 group (Fig. 6F and G). The decrease in the phosphorylated-AKT1 level in the ST2825 group compared with the negative control groups was partially reversed in the other two groups (Fig. 6H and I). The increase in the p21 level in the ST2825 group compared with the negative control groups was partially reversed in the ST2825 after IL-1α group, but not in the ST2825 + AKT1 group (Fig. 6J and K). These results were all consistent with those obtained *in vitro*.

Discussion

Previous studies have demonstrated that MyD88 plays a divergent role in carcinogenesis, with previous studies reporting that MyD88 contributes to the spontaneous tumorigenesis of skin and colon cancer (36,37); however, MyD88 has also been shown to be protective in virus-induced carcinogenesis (38). From the data obtained from TCGA, no significant difference was observed in the expression of MyD88 between most tumors and their adjacent tissues, such as breast cancer, lung cancer and prostate cancer; the expression of MyD88 in a few tumors was significantly lower than that in adjacent tumors, including diffuse large cell lymphoma, renal chromophobe cell tumor and thymic carcinoma; there were also a few tumors in which the expression of MyD88 was significantly higher than that near the tumor, such as the topic of the present study, PDAC (Fig. S1). In the present study, it was found that the inhibition of MyD88 by ST2825 induced the G2/M cell cycle arrest and apoptosis of PDAC cells. The expression of MyD88 in a pancreatic cancer chip was detected in pancreatic cancer and its adjacent tissues. The results revealed that the expression level of MyD88 in PDAC tissues was significantly higher than that in adjacent normal tissues, which was consistent with the aforementioned research results. In addition, according to the

level of MyD88 expression in HCC, a previous study divided the patients with HCC into a MyD88 high expression group and low expression group (25). The results revealed that the proportion of HCC in phase III-IV and the recurrence rate following surgery in the MyD88 high expression group was significantly higher; in addition, the overall survival rate and disease-free survival rate at 1, 3 and 5 years after surgery were much lower than that in the MyD88 low expression group. This suggests that the expression of MyD88 may be a potential prognostic indicator for patients with liver cancer (25). The present study found that in pancreatic cancer, patients with a high expression of MyD88 had a larger tumor volume and a shorter survival rate, suggesting that MyD88 may also be a potential prognostic indicator for patients with pancreatic cancer.

Previous research has indicated that ST2825, a selective inhibitor of MyD88, significantly inhibits the proliferation of liver cancer cells and promotes the apoptosis of HepG-2 in a concentration-dependent manner (29). Loiarro *et al* (28) found that ST2825 suppressed the inflammatory reaction via the MyD88/IRAK/NF-κB signaling pathway. However, the specific mechanisms of the effects of ST2825 on MyD88 in tumors were not verified. In the present study, it was found that in pancreatic cancer, ST2825 inhibited the function of MyD88 by inhibiting the dimerization of MyD88, which is consistent with previous extra-tumor research results (28).

The MyD88 signaling pathway, most often associated with IL-1R and TLR, regulates the pro-inflammatory feedback mechanism, participates in the tissue repair response and activates oncogenes. In tumors, the effects of MyD88 on tumor progression are mediated through TLR/IL-1R-dependent and -independent mechanisms. As previously demonstrated, in a TLR/IL-1R-dependent manner, MyD88 is activated following stimulation by lipopolysaccharide and IL-1, and plays a role in the activation of NF-κB, p38 or other pathways through changes in downstream tumor regulatory factors, such as MMP7, COX2, IL-6 and TNF-a (37,39). It has also been shown that, in a TLR/IL-1R-independent manner, in the process of RAS-mediated tumorigenesis, the MyD88 mutation interacted with ERK rather than IRAK, leading to the loss of its ability to regulate cell transformation (40).

Previous studies have indicated that MyD88, as a common intermediate messenger between NF-κB and its inducers, may constitute a novel therapeutic target for PDAC (18-20). Consistent with this finding, the present study demonstrated that ST2825 effectively inhibited PDAC development via the NF-κB/AKT1/p21 pathway in a TLR/IL-1R-dependent manner. The results indicated that the inhibition of the NF-κB pathway constituted the main mechanism of ST2825, as the process of NF-κB acting as a classic transcription factor family (including phosphorylation, nuclear import, specific DNA binding and downstream gene expression) was affected by ST2825.

As a classical transcription factor, NF-κB can play a role in tumors by regulating a variety of downstream targeted genes. A previous study found that ST2825 inhibited the NF-κB-mediated transcription and translation of cyclin-D1 in HCC (29). In the present study, according to the results of transcriptome sequencing and a NF-κB phosphorylation chip, AKT1 and cyclin-related genes were used as the main potential target factors. The results revealed that ST2825 induced severe G2/M cell cycle arrest; however, its key factor, the Cdk1-Cyclin B1 complex, did not exhibit any corresponding change, although the protein level of Cdk1 was reduced and the ratio of p-Cdk1/Cdk1 was slightly increased, which led to the decrease in the Cdk1-Cyclin B1 complex; the decreased level of the Cdk1-Cyclin B1 complex was not solely responsible however, for the range of G2/M cell cycle arrest. Thus, it was hypothesized that other factors were involved and played a decisive role. It was found that following ST2825 treatment, p21, which was known as an inhibitor of cell cycle progression that acting in the nucleus (41,42), was increased significantly. It is known that p21 is a classic downstream factor of p53, which can block the G2 to M phase transition; however, in the present study, the elevation of p21 was accompanied with a decrease in p53 expression, which indicated that p21 expression was increased by ST2825 in a p53-independent manner. According to the results of transcriptome sequencing, the mRNA level of p53 was not altered following treatment with ST2825 (Table SIII); it was thus speculated that ST2825 may affect the protein stability of p53, although the expression of MDM2 (Table SIII), which is known as a pro-degradation factor of p53 was also not altered. Thus, the detailed mechanism responsible for the decrease in p53 expression remains unclear, and this warrants further investigation. In addition, p21 expression increased following ST2825 treatment in the nuclear extracts, but decreased in the cytoplasmic extracts with a decrease in AKT1 expression. Together, these data indicated that ST2825 inhibited NF-κB transcriptional activity to increase p21 expression and promote its nuclear localization through the decreased expression of AKT1, which resulted in Cdk1-Cyclin B1 complex inhibition, thereby inducing G2/M cell cycle arrest and subsequent apoptosis.

The results of subsequent rescue experiments revealed that the addition of IL-1α, the overexpression of AKT1 or the knockdown of p21 partially inhibited the pro-apoptotic effects of ST2825. As regards IL-1α treatment, we found that the addition of 10 ng/ml IL-1α after ST2825 or simultaneously with ST2825 (5 μmol/l) did not reverse the effects of ST2825; however, when IL-1α was added prior to ST2825 treatment, it partially reversed the pro-apoptotic effects of ST2825, indicating that IL-1α was a upstream factor of MyD88 in the NF-κB pathway (Fig. S5). From these results, the authors also wished to determine whether the addition of IL-1α with ST2825 by intraperitoneally injection would also not be effective in *in vivo* experiments. For this purpose, the cells in the 'ST after IL-1α' group were incubated with 10 ng/ml IL-1α for 1 week before the injection to simulate a NF-κB activated model. Before the *in vivo* experiment, the *in vitro* preliminary experiment revealed that NF-κB was effectively activated by treatment with 10 ng/ml IL-1α for 1 week (Fig. S5). The model was successful. Furthermore, the results of western blot analysis demonstrated that IL-1α increased the level of phosphorylated p65 and phosphorylated akt1, and reduced the expression of p21. However, the overexpression of AKT1 did not affect the phosphorylation level of p65 and the expression of p21. In addition, the knockdown of p21 did not affect the activation level of p65 and akt1. These results clarified the upstream and downstream relationship of these factors.

In summary, pro-inflammatory factors, such as IL-1α activate the transcriptional activity of NF-κB through MyD88 in PDAC, thus regulating downstream factors (AKT1 and p21) to play a role in promoting tumor growth. ST2825 can block this process by inhibiting the dimerization of MyD88.

However, the present study had some limitations. As ST2825 is not an FDA-approved therapeutic drug, the effects of MyD88 inhibitor could not be confirmed in clinical trials. The detailed mechanisms responsible for the decrease in p53 expression induced by ST2825 are unclear and further investigations are thus required for clarifications. In addition, more practical animal models are warranted to verify the experimental results *in vitro*; thus, further studies are warranted.

In conclusion, the present study demonstrates that ST2825 induces the G2/M cell cycle arrest and apoptosis of PDAC cells via the MyD88/NF-κB/AKT1/p21 pathway. MyD88 may serve as a potential therapeutic target in PDAC. ST2825 may serve as a novel agent for the targeted therapy of PDAC in the future.

Acknowledgements

Not applicable.

Funding

The present study was supported by the Natural Science Foundation of Zhejiang Province (grant no. LY22H160017) and the Medical Science and Technology Foundation of Zhejiang Province (grant no. 2020KY751).

Availability of data and materials

The datasets used and/or analyzed during the current study are available from the corresponding author on reasonable request.

Authors' contributions

SL, TH, BZ, QZ and SY were involved in the conception and design of the study. SL and YZ were involved in the development of study methodology. SL TH and YZ were involved in the acquisition of data. SL and YZ were involved in the analysis and interpretation of data. SL, BZ and QZ were involved in the writing, reviewing and/or revision of the manuscript. BZ, QZ and SY were involved in the administrative, technical, or material support aspects of the study. YS supervised the study. All authors have read and approved the final manuscript. SL, TH and SY confirm the authenticity of all the raw data.

Ethics approval and consent to participate

All animal experiments were approved by the Zhejiang Medical Experimental Animal Care Commission and the Ethics Committee of the Second Affiliation Hospital of Zhejiang University School of Medicine. All procedures performed of the tissue ship involving human participants were approved by the Shanghai Qutdo Biotech Company Ethics Committee.

Patient consent for publication

Not applicable.

Competing interests

The authors declare that they have no competing interests.

References

1. Saluja A and Maitra A: Pancreatitis and pancreatic cancer. Gastroenterology 156: 1937-1940, 2019.
2. Neoptolemos JP, Kleeff J, Michl P, Costello E, Greenhalf W and Palmer DH: Therapeutic developments in pancreatic cancer: Current and future perspectives. Nat Rev Gastroenterol Hepatol 15: 333-348, 2018.
3. Mizrahi JD, Surana R, Valle JW and Shroff RT: Pancreatic cancer. Lancet 395: 2008-2020, 2020.
4. Siegel RL, Miller KD, Fuchs HE and Jemal A: Cancer statistics, 2022. CA Cancer J Clin 72: 7-33, 2022.
5. Matsuoka T and Yashiro M: Molecular targets for the treatment of pancreatic cancer: Clinical and experimental studies. World J Gastroenterol 22: 776-789, 2016.
6. Rozenblum E, Schutte M, Goggins M, Hahn SA, Panzer S, Zahurak M, Goodman SN, Sohn TA, Hruban RH, Yeoet CJ, *et al*: Tumor-suppressive pathways in pancreatic carcinoma. Cancer Res 57: 1731-1734, 1997.
7. Yashiro M, Carethers JM, Laghi L, Saito K, Slezak P, Jaramillo E, Rubio C, Koizumi K, Hirakawa K and Boland CR: Genetic pathways in the evolution of morphologically distinct colorectal neoplasms. Cancer Res 61: 2676-2683, 2001.
8. Moskaluk CA, Hruban RH and Kern SE: p16 and K-ras gene mutations in the intraductal precursors of human pancreatic adenocarcinoma. Cancer Res 57: 2140-2143, 1997.
9. Hruban RH, van Mansfeld AD, Offerhaus GJ, van Weering DH, Allison DC, Goodman SN, Kensler TW, Bose KK, Cameron JL and Bos JL: K-ras oncogene activation in adenocarcinoma of the human pancreas. A study of 82 carcinomas using a combination of mutant-enriched polymerase chain reaction analysis and allele-specific oligonucleotide hybridization. Am J Pathol 143: 545-554, 1993.
10. Kosmidis C, Sapalidis K, Kotidis E, Mixalopoulos N, Zarogoulidis P, Tsavlis D, Baka S, Man YG and Kanellos J: Pancreatic cancer from bench to bedside: Molecular pathways and treatment options. Ann Transl Med 4: 165, 2016.
11. Bryant KL, Mancias JD, Kimmelman AC and Der CJ: KRAS: Feeding pancreatic cancer proliferation. Trends Biochem Sci 39: 91-100, 2014.
12. Prabhu L, Mundade R, Korc M, Loehrer PJ and Lu T: Critical role of NF-κB in pancreatic cancer. Oncotarget 5: 10969-10975, 2014.
13. Wang W, Abbruzzese JL, Evans DB, Larry L, Cleary KR and Chiao PJ: The nuclear factor-kappa B RelA transcription factor is constitutively activated in human pancreatic adenocarcinoma cells. Clin Cancer Res 5: 119-127, 1999.
14. Fujioka S, Sclabas GM, Schmidt C, Frederick WA, Dong QG, Abbruzzese JL, Evans DB, Baker C and Chiao PJ: Function of nuclear factor kappaB in pancreatic cancer metastasis. Clin Cancer Res 9: 346-354, 2003.
15. Mo W, Chen J, Patel A, Zhang L, Chau V, Li YJ, Cho WS, Lim K, Xu J, Lazar AJ, *et al*: CXCR4/CXCL12 mediate autocrine cell-cycle progression in NF1-associated malignant peripheral nerve sheath tumors. Cell 152: 1077-1090, 2013.
16. Oeckinghaus A and Ghosh S: The NF-kappaB family of transcription factors and its regulation. Cold Spring Harb Perspect Biol 4: a000034. 2009.
17. Karandish F and Mallik S: Biomarkers and targeted therapy in pancreatic cancer. Biomarkers Cancer 8 (Suppl 1): S27-S35, 2016.
18. Takahashi H, Funahashi H, Sawai H, Matsuo Y, Yamamoto M, Okada Y, Takeyama H and Manabe T: Synthetic serine protease inhibitor, gabexate mesilate, prevents nuclear factor-kappaB activation and increases TNF-alpha-mediated apoptosis in human pancreatic cancer cells. Dig Dis Sci 52: 2646-2652, 2007.
19. Zhuang Z, Ju HQ, Aguilar M, Gocho T, Li H, Iida T, Lee H, Fan X, Zhou H, Ling J, *et al*: IL1 receptor antagonist inhibits pancreatic cancer growth by abrogating NF-κB activation. Clin Cancer Res 22: 1432-1444, 2016.
20. Sun YL, Wu CS, Ma JX, Yang Y, Man XH, Wu HY and Li SD: Toll-like receptor 4 promotes angiogenesis in pancreatic cancer via PI3K/AKT signaling. Exp Cell Res 347: 274-282, 2016.

21. Niu J, Li Z, Peng B and Chiao PJ: Identification of an autoregulatory feedback pathway involving interleukin-1a in induction of constitutive NF-kappaB activation in pancreatic cancer cells. J Biol Chem 279: 16452-16462, 2004.
22. Ling JH, Kang Y, Zhao RY, Xia QH, Lee DF, Chang Z, Li J, Peng BL, Fleming JB, Wang HM, *et al*: KrasG12D-Induced IKK2/β/NF-κB activation by IL-1α and p62 feedforward loops is required for development of pancreatic ductal adenocarcinoma. Cancer Cell 21: 105-120, 2012.
23. Zhang DX, Li L, Jiang HM, Knolhoff BL, Lockhart AC, Wang-Gillam A, DeNardo DG, Ruzinova MB and Lim KH: Constitutive IRAK4 activation underlies poor prognosis and chemoresistance in pancreatic ductal adenocarcinoma. Clin Cancer Res 23: 1748-1759, 2017.
24. Salcedo R, Cataisson C, Hasan U, Yuspa SH and Trinchieri G: MyD88 and its divergent toll in carcinogenesis. Trends Immunol 34: 232-238, 2013.
25. Liang B, Chen R, Wang T, Cao L, Liu Y, Yin F, Zhu M, Fan X, Liang Y, Zhang L, *et al*: Myeloid differentiation Factor 88 promotes growth and metastasis of human hepatocellular carcinoma. Clin Cancer Res 19: 2905-2915, 2013.
26. Song B, Zhang C, Li G, Jin G and Liu C: MiR-940 inhibited pancreatic ductal adenocarcinoma growth by targeting MyD88. Cell Physiol Biochem 35: 1167-1177, 2015.
27. Zhu XX, Burfeind KG, Michaelis KA, Braun TP, Olson B, Pelz KR, Morgan TK and Marks DL: MyD88 signalling is critical in the development of pancreatic cancer cachexia. J Cachexia Sarcopeni 10: 378-390, 2019.
28. Loiarro M, Capolunghi F, Fantò N, Gallo G, Campo S, Arseni B, Carsetti R, Carminati P, Santis RD, Ruggiero V, *et al*: Pivotal advance: Inhibition of MyD88 dimerization and recruitment of IRAK1 and IRAK4 by a novel peptidomimetic compound. J Leukoc Biol 82: 801-810, 2007.
29. Deng Y, Sun J and Zhang LD: Effect of ST2825 on the proliferation and apoptosis of human hepatocellular carcinoma cells. Genet Mol Res 15: 15016826, 2016.
30. Livak KJ and Schmittgen TD: Analysis of relative gene expression data using real-time quantitative PCR and the 2(-Delta Delta C(T)) method. Methods 25: 402-408, 2001.
31. Van Tassell BW, Seropian IM, Toldo S, Salloum FN, Smithson L, Varma A, Hoke NN, Gelwix C, Chau V and Abbate A: Pharmacologic inhibition of myeloid differentiation factor 88 (MyD88) prevents left ventricular dilation and hypertrophy after experimental acute myocardial infarction in the mouse. J Cardiovasc Pharmacol 55: 385-390, 2020.
32. Jiang S, Li F, Li X, Wang L, Zhang L, Lu C, Zheng L and Yan M: Transcriptome analysis of PK-15 cells in innate immune response to porcine deltacoronavirus infection. PLoS One 14: e0223177, 2019.
33. Rinaldi L, Delle DR, Catalanotti B, Torres-Quesada O, Enzler F, Moraca F, Nisticò R, Chiuso F, Piccinin S, Bachmann V, *et al*: Feedback inhibition of cAMP effector signaling by a chaperone-assisted ubiquitin system. Nat Commun 10: 2572, 2019.
34. Liu D, Li L, Zhang XX, Wan DY, Xi BX, Hu Z, Ding WC, Zhu D, Wang XL, Wang W, *et al*: SIX1 promotes tumor lymphangiogenesis by coordinating TGFβ signals that increase expression of VEGF-C. Cancer Res 74: 5597-5607, 2014.
35. Ignacio RMC, Dong YL, Kabir SM, Choi H, Lee E, Wilson AJ, Beeghly-Fadiel A, Whalen MM and Son D: CXCR2 is a negative regulator of p21 in p53-dependent and independent manner via Akt-mediated Mdm2 in ovarian cancer. Oncotarget 9: 9751-9765, 2018.
36. Mittal D, Saccheri F, Vénéreau E, Pusterla T, Bianchi ME and Rescigno M: TLR4-mediated skin carcinogenesis is dependent on immune and radioresistant cells. EMBO J 29: 2242-2252, 2010.
37. Rakoff-Nahoum S and Medzhitov R: Regulation of spontaneous intestinal tumorigenesis through the adaptor protein MyD88. Science 317: 124-127, 2007.
38. Fathallah I, Parroche P, Gruffat H, Zannetti C, Johansson H, Yue J, Manet E, Tommasino M, Sylla BS and Hasan UA: EBV latent membrane protein 1 is a negative regulator of TLR9. J Immunol 185: 6439-6447, 2010.
39. Naugler WE, Sakurai T, Kim S, Maeda S, Kim K, Elsharkawy AM and Karin M: Gender disparity in liver cancer due to sex differences in MyD88-dependent IL-6 production. Science 317: 121-124, 2007.
40. Coste I, Le Corf K, Kfoury A, Hmitou I, Druillennec S, Hainaut P, Eychene A, Lebecque S and Renno T: Dual function of MyD88 in RAS signaling and inflammation, leading to mouse and human cell transformation. J Clin Invest 120: 3663-3667, 2010.
41. Watanabe S, Yamaguchi S, Fujii N, Eguchi N, Katsuta H, Sugishima S, Iwasaka T and Kaku T: Nuclear Co-expression of p21 and p27 induced effective cell-cycle arrest in T24 cells treated with BCG. Cytotechnology 71: 219-229, 2019.
42. Chang XT, Chai ZB, Zou JR, Wang HX, Wang Y, Zheng YB, Wu H and Liu CY: PADI3 induces cell cycle arrest via the Sirt2/AKT/p21 pathway and acts as a tumor suppressor gene in colon cancer. Cancer Biol Med 16: 729-742, 2019.